arXiv:cond-mat/0103299v1 [cond-mat.stat-mech] 14 Mar 2001

Vortices in a rotating Bose-Einstein condensate: critical velocities and energy diagrams in the Thomas-Fermi regime

Amandine Aftalion*
Laboratoire d'analyse numérique, B.C.187, Université Paris 6, 175 rue du Chevaleret, 75013 Paris, France.

Qiang Du†
Department of Mathematics, Iowa State University, Ames, IA 50011, USA.

(Dated: February 1, 2008)

For a Bose-Einstein condensate placed in a rotating trap and confined in the z axis, we set a framework of study for the Gross-Pitaevskii energy in the Thomas Fermi regime. We investigate an asymptotic development of the energy, the critical velocities of nucleation of vortices with respect to a small parameter ε and the location of vortices. The limit ε going to zero corresponds to the Thomas Fermi regime. The non-dimensionalized energy is similar to the Ginzburg-Landau energy for superconductors in the high-kappa high-field limit and our estimates rely on techniques developed for this latter problem. We also take the advantage of this similarity to develop a numerical algorithm for computing the Bose-Einstein vortices. Numerical results and energy diagrams are presented.

PACS numbers: 03.75.Fi,02.70.-c

I. INTRODUCTION

Since the first experimental achievement of Bose-Einstein condensates in atomic gases in 1995, many properties of these systems have been studied experimentally and theoretically, and particularly the existence of vortices [1, 2, 3, 4, 5, 6, 7, 8]. A way to create vortices consists in rotating the trap confining the atoms: for sufficiently large velocities, it becomes energetically favorable to have vortices in the system. Theoretical studies of this type of experiments have often been made in the framework of the nonlinear Schrödinger equation or Gross-Pitaevskii equation, well known for superfluids, but which provides a very good description of Bose-Einstein condensates: it is assumed that the N particles of the gas are condensed in the same state for which the wave function ϕ minimizes the Gross-Pitaevskii energy. By introducing a rotating frame at the angular velocity $\tilde{\mathbf{\Omega}} = \tilde{\Omega}\mathbf{e}_z$, the trapping potential becomes time independent, and the wave function ϕ minimizes the energy

$$\mathcal{E}_{3D}(\phi) = \int \frac{\hbar^2}{2m}|\nabla\phi|^2 + \frac{m}{2}\sum_\alpha \omega_\alpha^2 r_\alpha^2 |\phi|^2 + \frac{N}{2} g_{3D}|\phi|^4 - \hbar\tilde{\mathbf{\Omega}}\cdot(i\phi, \nabla\phi\times\mathbf{x}), \quad (1)$$

under the constraint $\int|\phi|^2 = 1$. Here, for any complex quantities u and v and their complex conjugates $\bar{u}$ and $\bar{v}$, $(u,v) = (u\bar{v}+\bar{u}v)/2$. The terms in the energy correspond to the kinetic energy, the trapping potential energy, the interaction energy and the inertial due to the change of frame.

When the atoms are strongly confined in the $z-$axis, the situation can be simplified to a two dimensional problem where the wave function ψ depends only on $\mathbf{x} = (x,y)$ and it minimizes

$$\mathcal{E}_{2D}(\psi) = \int \frac{\hbar^2}{2m}|\nabla\psi|^2 + \frac{m}{2}\sum_{\alpha=x,y} \omega_\alpha^2 r_\alpha^2 |\psi|^2 + \frac{N}{2} g|\psi|^4 - \hbar\tilde{\mathbf{\Omega}}\cdot(i\psi, \nabla\psi\times\mathbf{x}), \quad (2)$$

where $g = g_{3D}(m\omega_z/2\pi\hbar)$. The constraint $\int|\psi|^2 = 1$ is also imposed. Our study was at first motivated by the work of Castin and Dum [2] who have studied the equilibrium configurations by looking for the minimizers in a reduced class of functions for the 2D case and have done numerical computations in 2 and 3D. Their analysis is in the Thomas-Fermi regime, where the mean interaction energy per particle is larger than $\hbar\omega_{x,y}$.

Our aim is to provide a mathematical framework for a rigorous study of the energy $\mathcal{E}_{2D}$ and its minimizers in the Thomas Fermi limit. We first observe that this energy has a striking similarity with the high-kappa, high-field limit of the Ginzburg-Landau free energy used in the modeling of superconductors. Thus, we expect the energy $\mathcal{E}_{2D}$ will develop similar behavior as those for the Ginzburg-Landau energy studied in [11, 12, 13]. In particular, the results obtained in the context of Ginzburg-Landau energy may be applied to $\mathcal{E}_{2D}$, in the Thomas Fermi regime, to yield an asymptotic development of the energy as well as the critical velocities for the nucleation of vortices and the location of these vortices. Due to the close resemblance, we will not be concerned with the detailed derivations in this paper, but rather focus on the conclusions one can draw from the asymptotic developments. To our knowledge, some of our estimates to be presented later have not been given in the literature previously. Let us point out that our method to compute the energy is also new in this context and very different

*Electronic address: aftalion@ann.jussieu.fr
†Also at the Department of Mathematics, Hong Kong University of Science and Technology, Clear Water Bay, Hong Kong; Electronic address: qdu@iastate.edu

from the ones in, for instance, [2, 4, 8].

We define the characteristic length $d = (\hbar/m\omega_x)^{1/2}$ and set

$$\varepsilon^2 = \frac{\hbar^2}{2Ngm}.$$

In the Thomas-Fermi approximation, ε is small, which will be our asymptotic regime. We re-scale the distance by $R = d/\sqrt{\varepsilon}$ and define $u(\mathbf{r}) = R\psi(\mathbf{x})$ where $\mathbf{x} = R\mathbf{r}$. Assume that $\omega = \omega_x$ and $\omega_y = \lambda\omega$ with $0 \leq \lambda \leq 1$ and we set $\Omega = \tilde{\Omega}/\varepsilon\omega$. Since the trapping potential is stronger than the inertial potential, we have $\Omega < 1/\varepsilon$. The energy can be rewritten as:

$$\begin{aligned} E_{2D}(u) &= \int \frac{1}{2}|\nabla u|^2 + \frac{1}{2\varepsilon^2}(x^2+\lambda^2 y^2)|u|^2 + \frac{1}{4\varepsilon^2}|u|^4 \\ &\quad + \mathbf{\Omega}\cdot(iu, \nabla u \times \mathbf{r})\ . \end{aligned} \tag{3}$$

Due to the constraint $\int |u|^2 = 1$, we can add to E_{2D} any multiple of $\int |u|^2$ so that it is equivalent to minimize

$$\int |\nabla u|^2 + 2\mathbf{\Omega}\cdot(iu, \nabla u \times \mathbf{r}) + \frac{1}{2\varepsilon^2}|u|^4 - \frac{1}{\varepsilon^2}a(\mathbf{r})|u|^2$$

where $a(\mathbf{r}) = \alpha - (x^2 + \lambda^2 y^2)$ for some constant α to be determined. Let $\mathcal{D}$ be the ellipse $\{a > 0\} = \{x^2 + \lambda^2 y^2 < \alpha\}$. We impose the following constraint on α:

$$\int_{\mathcal{D}} a(\mathbf{r}) = 1. \tag{4}$$

Indeed, as ε tends to 0, the minimizer will satisfy that $|u|^2$ will be close to a so that the constraint will be satisfied automatically by u if we impose (4). Equation (4) leads to $\alpha^2 = 2\lambda/\pi$. If $\lambda = 1$, that is $\omega_x = \omega_y$, then $\mathcal{D}$ is a disc of radius R_0 with $R_0^4 = 2/\pi$.

To study the problem analytically, it is reasonable to minimize the energy over the domain $\mathcal{D}$ with zero boundary data for u. Indeed, when $a \leq 0$, the energy is convex so that the minimizer u goes to zero exponentially at infinity (see the numerical observation in [2] and the analysis on the behavior near the boundary of $\mathcal{D}$ as well as the decay at infinity of the order parameter in [9, 10]). Denote $H^m(\mathcal{D})$ the space of square integrable functions defined on the domain $\mathcal{D}$ that have square integrable derivatives up to the order m, and $H_0^1(\mathcal{D})$ the space of functions in $H^1(\mathcal{D})$ satisfying the zero boundary condition. Denote the norm $\left(\int_{\mathcal{D}} |v|^2\right)^{1/2}$ by $\|v\|$ for any square integrable function v, we then consider the problem

$$\min E_\varepsilon(u) \ \text{ subject to } \ u \in H_0^1(\mathcal{D}),\ \|u\| = 1 \tag{P}$$

where

$$\begin{aligned} E_\varepsilon(u) &= \int_{\mathcal{D}} |\nabla u|^2 + 2\mathbf{\Omega}\cdot(iu, \nabla u \times \mathbf{r}) \\ &\quad + \frac{1}{2\varepsilon^2}(a(\mathbf{r}) - |u|^2)^2. \end{aligned} \tag{5}$$

Note that critical point u of E_ε is a solution of

$$-\Delta u - 2i(\mathbf{\Omega}\times\mathbf{r}).\nabla u = \frac{1}{\varepsilon^2}u(a - |u|^2) + \mu_\varepsilon u \text{ in } \mathcal{D}, \tag{6}$$

with $u = 0$ on $\partial\mathcal{D}$ and μ_ε is the Lagrange multiplier. The specific choice of α in (4) will imply that the term $\mu_\varepsilon u$ is negligible in front of au/ε^2.

We want to study the behavior of $\min E_\varepsilon(u)$ as ε goes to 0. In Section 2, we compute an asymptotic development of the energy and in Section 3, the critical velocities of nucleation of vortices and the location of the vortices. In Section 4, we study the evolution in imaginary time and construct some numerical algorithms. In Section 5, we present some computational results and the energy diagrams.

II. ASYMPTOTIC DEVELOPMENT OF THE ENERGY

To study the behavior of the minimizer of the energy when ε goes to zero, we observe that the form of the energy (5) is close to the Ginzburg-Landau functional studied in [11], [12] where the magnetic field has been replaced by a rotating term and similar to [13] except for the trapping potential and the minimization over constraint. The main idea is to decouple the energy into three terms: a part coming from the solution without vortices, a vortex contribution and a term due to rotation. The estimate on the vortex contribution was developed in [12, 13, 14, 15].

A. The solution without vortices

Firstly, we are interested in solutions without vortices, that is u has no zero in the interior of $\mathcal{D}$. Thus we consider functions of the form $\eta = fe^{iS}$, where η is in $H_0^1(\mathcal{D})$ and f is real and has no zero in the interior of $\mathcal{D}$. We consider first minimizing E_ε over such functions without imposing the constraint that the L^2 norm is 1, that is, f and S minimize

$$\begin{aligned} \mathcal{E}_\varepsilon(f, S) &= \int_{\mathcal{D}} |\nabla f|^2 + \frac{1}{2\varepsilon^2}(a - f^2)^2 \\ &\quad + \int f^2|\nabla S - \mathbf{\Omega}\times\mathbf{r}|^2 - f^2\Omega^2 r^2. \end{aligned} \tag{7}$$

We have $f = 0$ on $\partial\mathcal{D}$ and

$$-\Delta f + f\nabla S(\nabla S - 2\mathbf{\Omega}\times\mathbf{r}) = \frac{1}{\varepsilon^2}f(a - f^2) \text{ in } \mathcal{D}, \tag{8}$$

$$\operatorname{div}(f^2(\nabla S - \mathbf{\Omega}\times\mathbf{r})) = 0. \tag{9}$$

Equation (9) implies that there exists ξ in $H^2(\mathcal{D}) \cap H_0^1(\mathcal{D})$ such that

$$f^2(\nabla S - \mathbf{\Omega}\times\mathbf{r}) = \Omega\nabla^\perp\xi, \tag{10}$$

where $\nabla^\perp\xi = (-\partial_y\xi, \partial_x\xi)$. So ξ is the unique solution of

$$\mathrm{div}(\frac{1}{f^2}\nabla\xi) = 0 \text{ in } \mathcal{D}, \quad \xi = 0 \text{ on } \partial\mathcal{D}. \tag{11}$$

Note that equation (10) is the equation for the velocity, but we prefer to write it as an orthogonal gradient for our later purposes of integration by part. In the special case where $\mathcal{D}$ is a disc, the minimum of (7) is reached for $\nabla S = 0$ but this is not the case if $\mathcal{D}$ is an ellipse and there is a non trivial solution of (9).

a. The case of the disc Assume that $\lambda = 1$ so that $\mathcal{D}$ is a disc and $a(r) = R_0^2 - r^2$. As discussed earlier, $\nabla S = 0$ in this case so that the energy becomes

$$\mathcal{E}_\varepsilon(f) = \int_{\mathcal{D}} |\nabla f|^2 + \frac{1}{2\varepsilon^2}(a(r) - f^2)^2. \tag{12}$$

Let η_ε be the minimizer of (12) over real valued functions in $H_0^1(\mathcal{D})$. Then, η_ε has no vortex, is independent of Ω and satisfies

$$\Delta\eta_\varepsilon = \frac{1}{\varepsilon^2}\eta_\varepsilon(\eta_\varepsilon^2 - a) \text{ in } \mathcal{D}, \quad \eta_\varepsilon = 0 \text{ on } \partial\mathcal{D}.$$

When ε tends to 0, η_ε^2 is close to a except on a boundary layer of size $\varepsilon^{2/3}$ close to $\partial\mathcal{D}$. More precisely, using sub and super solutions, one can verify that

$$\sqrt{a(r)}\tanh(\delta(\sqrt{a(r)})^3|\log\,\varepsilon|) \le \eta_\varepsilon \le \sqrt{a(r)}$$

for $|R_0^2 - r^2| \ge C\varepsilon^{1/3}$. In fact, one can construct a sub solution of the type above in any region $|R_0^2 - r^2| \ge C\varepsilon^{\beta/3}$ with $\beta < 2$. Then the value of δ is less than $c(2-\beta)$.

The boundary layer can be analyzed using the change of variable $x = (R_0 - r)/\varepsilon^{2/3}$ and $v_\varepsilon(x) = \eta_\varepsilon(r)/\varepsilon^{2/3}$. Then v_ε satisfies the Painlevé equation

$$v'' = v(v^2 - 2R_0x), \;\; v(0) = 0, \;\; v(x) \simeq 2R_0x \;\text{ for } x \text{ large.}$$

The boundary behavior has already been studied in [10] and [9], but using matched asymptotics.

The energy of η_ε can also be estimated by a test function equal to $\sqrt{a}$ except on the boundary layer to get

$$E_\varepsilon(\eta_\varepsilon) \le \frac{2\pi}{3}|\log\,\varepsilon|(1 + o(1)). \tag{13}$$

b. The case of an ellipse As discussed before, the minimum $\eta_\varepsilon = f_\varepsilon e^{iS_\varepsilon}$ of (7) has a non-trivial phase. f_ε^2 tends to a in every compact subset of $\mathcal{D}$ and the function ξ_ε given by (10) or (11) tends to the unique solution ξ of

$$\mathrm{div}(\frac{1}{a}\nabla\xi) = 0 \text{ in } \mathcal{D}, \quad \xi = 0 \text{ on } \partial\mathcal{D}. \tag{14}$$

One can easily get that $\xi(x,y) = -a^2(x,y)/(2 + 2\lambda^2)$. Using (10), we can define S_0, the limit of S_ε, to be the solution of $a(\nabla S_0 - \mathbf{\Omega}\times\mathbf{r}) = \Omega\nabla^\perp\xi$ with zero value at the origin. We have $S_0 = C\Omega xy$ with $C = (\lambda^2 - 1)/(\lambda^2 + 1)$. We see that S_0 cancels when $\lambda = 1$ that is in the case of the disc. This computation is consistent with the one in [8], though it is derived in a different way.

B. Decoupling the energy

Let $\eta_\varepsilon = f_\varepsilon e^{iS_\varepsilon}$ be the vortex free minimizer of E_ε discussed previously without imposing the constraint on the norm of u. Let u_ε be a minimizer of E_ε under the constraint $\int_{\mathcal{D}} |u|^2 = 1$ and let $v_\varepsilon = u_\varepsilon/\eta_\varepsilon$. Since η_ε satisfies the Gross Pitaevskii equation (8)-(9), we have

$$\int_{\mathcal{D}} (|v|^2 - 1)(-\frac{1}{2}\Delta f_\varepsilon^2 - \frac{1}{\varepsilon^2}f_\varepsilon^2(a - f_\varepsilon^2) + |\nabla f_\varepsilon e^{iS_\varepsilon}|^2 - 2f_\varepsilon^2(\nabla S_\varepsilon \cdot \mathbf{\Omega}\times\mathbf{r}) = 0.$$

Using this identity, one can get that the energy $E_\varepsilon(u_\varepsilon)$ decouples as follows

$$E_\varepsilon(u_\varepsilon) = E_\varepsilon(\eta_\varepsilon) + G_\varepsilon(v_\varepsilon) + 2\int_{\mathcal{D}} |\eta_\varepsilon|^2(\nabla S_\varepsilon - \mathbf{\Omega}\times\mathbf{r})\cdot(iv_\varepsilon, \nabla v_\varepsilon), \tag{15}$$

where

$$G_\varepsilon(v_\varepsilon) = \int_{\mathcal{D}} |\eta_\varepsilon|^2|\nabla v_\varepsilon|^2 + \frac{|\eta_\varepsilon|^4}{2\varepsilon^2}(1 - |v_\varepsilon|^2)^2.$$

This decoupling was used in [13] in the case of a disc where $\nabla S_\varepsilon = 0$.

C. Estimate on the energy

We now estimate the terms in (15). The first term $E_\varepsilon(\eta_\varepsilon)$ is a constant only depending on ε, and not on the solution type, that is with or without vortices. The second term gives a contribution coming from the vortices and the third term is due to the vortices and rotation.

We use the analysis of vortices developed in [14] and later in [12, 13, 15]. Let $\mathcal{D}'_\varepsilon = D \setminus \{x,\ \mathrm{dist}(x, \partial\mathcal{D}) \le \varepsilon^\beta\}$, with $\beta < 1$. Then in $\mathcal{D}'_\varepsilon$ it is possible to define vortices for v_ε in the following way: there exist balls $B_i = B(p_i, \varepsilon^{\beta'})$ where p_i are points in $\mathcal{D}'_\varepsilon$ at mutual distance bigger than $8\varepsilon^{\beta'}$ and $\beta' > \beta$, such that $|v_\varepsilon| \ge 1/2$ in $\mathcal{D}'_\varepsilon \setminus \cup_i B_i$. Moreover, the degree $d_i = deg(v_\varepsilon/|v_\varepsilon|, \partial B_i)$ is not zero and there is an estimate of the energy of v_ε in each ball B_i. This analysis means that vortices are in fact defined in the balls where v_ε is less than $1/2$ and has a non zero degree. This allows us to compute $G_\varepsilon(v_\varepsilon)$ for which only the gradient term in the vortex balls will give a contribution: each vortex gives a contribution in the amount of $2\pi|\log\,\varepsilon|$ due to its degree and a contribution of lower order which comes from the interaction with the other vortices. Moreover, $|\eta_\varepsilon|^2$ is almost a:

$$G_\varepsilon(v) = 2\pi|\log\,\varepsilon|\sum_i |d_i|a(p_i) - 2\pi\sum_{i\neq j} d_id_ja(p_i)a(p_j)\log|p_i - p_j| + O(1). \tag{16}$$

In order to estimate the third term in (15) we let X_ε be the solution of $a(\mathbf{r})(\nabla S_0 - \mathbf{\Omega}\times\mathbf{r}) = \Omega\nabla^\perp X_\varepsilon$ which is

zero on the boundary of $\mathcal{D}'_\varepsilon$. That is X_ε solves (14) but with zero boundary data on $\partial\mathcal{D}'_\varepsilon$ instead of $\partial\mathcal{D}$. Hence X_ε converges to ξ the solution of (14). An integration by part on the last term of (15) using the definition of X_ε and the definition of the degree of v_ε on vortex balls and the fact that the higher order term comes from an integration on the vortex balls yields

$$\begin{aligned}
&\int_{\mathcal{D}} |\eta_\varepsilon|^2(\nabla S_\varepsilon - \mathbf{\Omega}\times\mathbf{r})\cdot(iv,\nabla v)\\
&\quad=\int_{\mathcal{D}'_\varepsilon\setminus\cup_i B_i}\mathbf{\Omega}\cdot(iv,dX_\varepsilon\times\nabla v)(1+o(1))\\
&\quad=\sum_i 2\pi\Omega d_i X_\varepsilon(p_i)(1+o(1))\\
&=\sum_i\frac{-\pi\Omega d_i}{1+\lambda^2}(\alpha-|x_i|^2-\lambda^2|y_i|^2)^2(1+o(1))\,. \quad (17)
\end{aligned}$$

Finally, one can derive from (15)-(16)-(17) an asymptotic development of the energy for a solution with vortices.

$$\begin{aligned}
E_\varepsilon(u_\varepsilon)-E_\varepsilon(\eta_\varepsilon)&\simeq 2\pi|\log\varepsilon|\sum_i|d_i|a(p_i)\\
&-2\pi\sum_{i\neq j}d_id_ja(p_i)a(p_j)\log|p_i-p_j|\\
&-\frac{\pi\Omega}{1+\lambda^2}\sum_i d_i\Big(\alpha-|x_i|^2-\lambda^2|y_i|^2\Big)^2. \quad (18)
\end{aligned}$$

Note that the minimal energy for solutions without vortices in $\mathcal{D}'_\varepsilon$ is $E_\varepsilon(\eta_\varepsilon)+O(\varepsilon|\log\varepsilon|)$: it is not exactly $E_\varepsilon(\eta_\varepsilon)$ since η_ε is a minimizer without the constraint $\|\eta_\varepsilon\|=1$, but it almost equals to $E_\varepsilon(\eta_\varepsilon)$ since $\int_{\mathcal{D}} a = 1$ and $|\eta_\varepsilon|^2$ approaches a asymptotically.

III. CRITICAL VELOCITIES

A. Critical velocity for the existence of one vortex

Let u_ε be a minimizer of (P) with one vortex at a point p in $\mathcal{D}$ with coordinates (x,y) and let ΔE_ε be the difference between $E_\varepsilon(u_\varepsilon)$ and the energy of a solution without vortex $(E_\varepsilon(\eta_\varepsilon)+O(\varepsilon|\log\varepsilon|))$:

$$\begin{aligned}
\Delta E_\varepsilon &= 2\pi\Big(\alpha-x^2-\lambda^2y^2\Big)\cdot\\
&\Big(|\log\varepsilon|-\frac{\Omega}{1+\lambda^2}(\alpha-x^2-\lambda^2y^2)\Big)(1+o(1)). \quad (19)
\end{aligned}$$

This expression has been obtained by Svidzinsky and Fetter [8] using a different method. The form of ΔE_ε allows the computation of two critical velocities Ω_s and Ω_1 for the existence of vortices: Ω_s is the velocity for which the solution with one vortex starts to be locally stable and Ω_1 for which it starts to be globally stable. For $\Omega<\Omega_s$, ΔE_ε is a decreasing function of $|p|$, the position of the vortex; $|p|=0$ is a local maximum of ΔE_ε. For $\Omega_s<\Omega<\Omega_1$, $|p|=0$ is a local minimum for ΔE_ε. Note that $\Delta E_\varepsilon(p\in\partial D)=0$ and $\Delta E_\varepsilon(|p|=0)>0$.

For $\Omega>\Omega_1$, $|p|=0$ is the global minimum for ΔE_ε. :

$$\begin{aligned}
\Omega_s&=\frac{1+\lambda^2}{2\alpha}|\log\varepsilon|=\frac{1+\lambda^2}{4\sqrt{\lambda}}\sqrt{2\pi}|\log\varepsilon|\,,\\
\Omega_1&=\frac{1+\lambda^2}{\alpha}|\log\varepsilon|=\frac{1+\lambda^2}{2\sqrt{\lambda}}\sqrt{2\pi}|\log\varepsilon|
\end{aligned}$$

that is

$$\tilde\Omega_s=\frac{1+\lambda^2}{4\sqrt{\lambda}}\omega\sqrt{\frac{\pi\hbar^2}{Ngm}}\log\Big(\frac{Ngm}{\hbar^2}\Big)^{1/2},$$

$$\tilde\Omega_1=\frac{1+\lambda^2}{2\sqrt{\lambda}}\omega\sqrt{\frac{\pi\hbar^2}{Ngm}}\log\Big(\frac{Ngm}{\hbar^2}\Big)^{1/2}.$$

Note that Castin-Dum [2] for the case $\lambda=1$ find $\tilde\Omega_1=\omega\sqrt{(\pi\hbar^2)/(Ngm)}\log\Big((C/\sqrt{\pi})(Ngm)/\hbar^2\Big)^{1/2}$, with $C\simeq 1.8$, hence $C/\sqrt{\pi}\simeq 1$ which gives a value of $\tilde\Omega_1$ very close to ours. They also have $\Omega_1=2\Omega_s$ for the case $\lambda=1$. Increases in anisotropy yield higher $\tilde\Omega_1$ as already noticed in [4], but as λ tends to infinity, Ω_1 becomes bigger than $1/\varepsilon$ so that vortices cannot be stabilized.

It can be proved that there exists k_ε which tends to zero with ε such that for $\Omega<\Omega_1-k_\varepsilon$, the minimizer of E_ε has no vortex and for $\Omega>\Omega_1+k_\varepsilon$, there exists a minimizer with a vortex. Moreover, for $\Omega_1+k_\varepsilon<\Omega<\Omega_1+O(1)$, any minimizer has one vortex of degree 1 tending to the origin. The proof consists in constructing a test function with a vortex at the origin and computing the energy of this test function. This yields an upper bound for the energy. The lower bound relies on estimates for $G_\varepsilon(v)$ from [14] and [12, 13].

B. Critical velocity for n vortices

Similarly, one can compute Ω_n, the critical velocity for the existence of n vortices. For this purpose, one can prove that as ε goes to 0, the vortices tend to the origin and they are of degree 1 that is $d_i=1$. This is similar to [12], [13]. The test function consists in putting the n vortices on a polygon centered at the origin of size $1/\sqrt{\Omega}$ in x and $1/\lambda\sqrt{\Omega}$ in y. More precisely, we let $\tilde p_i$ with coordinates $(\tilde x_i,\tilde y_i)$ be such that $\tilde x_i=x_i\sqrt{\Omega}$ and $\tilde y_i=\lambda y_i\sqrt{\Omega}$. This allows us to estimate the energy of a solution with n vortices centered at $\tilde p_i$ from (15),(16),(17):

$$\begin{aligned}
E_\varepsilon(u)&=E_\varepsilon(\eta_\varepsilon)+2\pi n\alpha(|\log\varepsilon|-\frac{1}{1+\lambda^2}\Omega\alpha)\\
&+\pi(n^2-n)\alpha^2\log\Omega+w(\tilde p_1,...,\tilde p_n)+C_n+o(1) \quad (20)
\end{aligned}$$

where C_n is a constant that depends on n and λ and

$$w(\tilde p_1,...,\tilde p_n)=-\pi\alpha^2\sum_{i\neq j}\log\Big(|\tilde x_i-\tilde x_j|^2+\frac{|\tilde y_i-\tilde y_j|^2}{\lambda^2}\Big)$$

$$+2\pi\alpha\sum_i(\tilde{x}_i^2+\tilde{y}_i^2)\Big(\frac{2}{1+\lambda^2}-\frac{|\log\,\varepsilon|}{\Omega\alpha}\Big). \tag{21}$$

Recall that $\alpha^2 = 2\lambda/\pi$. For fixed λ, w is of order 1, hence is of lower order than the previous terms. Then the critical velocity for the existence of n vortices can be computed from (20)

$$\Omega_n = (1+\lambda^2)\sqrt{\frac{\pi}{2\lambda}}|\log\,\varepsilon| + \frac{(1+\lambda^2)}{2}(n-1)\log\Big((1+\lambda^2)\sqrt{\frac{\pi}{2\lambda}}|\log\,\varepsilon|\Big), \tag{22}$$

and the critical velocity in the original parameters is $\tilde{\Omega}_n$

$$\tilde{\Omega}_n = \frac{(1+\lambda^2)}{2}\omega\Big(\sqrt{\frac{\pi\hbar^2}{Ngm\lambda}}\log\Big(\frac{Ngm}{\hbar^2}\Big)^{1/2} + (n-1)\sqrt{\frac{\hbar^2}{2Ngm}}\log\Big(\frac{1+\lambda^2}{2\sqrt{\lambda}}\sqrt{2\pi}\log(\frac{Ngm}{\hbar^2})^{1/2}\Big)\Big).$$

C. Location of vortices

Once Ω is close to Ω_n, the location of the vortices is characterized by the configuration of points $\{\tilde{p}_i\}$ which minimizes the function w given by (21). In non-dimensionalized variables, the points are given by $Rp_i/\sqrt{2\pi|\log\,\varepsilon|}$. For convenience, we define

$$\rho = \sqrt{\frac{2\pi}{\lambda}}\Big(\frac{2}{(1+\lambda^2)}-\frac{|\log\,\varepsilon|}{\Omega\alpha}\Big).$$

Note that given the value of Ω_n in (22), to leading order, ρ is equal to $\sqrt{2\pi/\lambda}/(1+\lambda^2)$. We use the value of α and ρ to get a simplified expression for w:

$$w(\tilde{p}_1,...,\tilde{p}_n) = -2\lambda\Big(\sum_{i\neq j}\log\Big(|\tilde{x}_i-\tilde{x}_j|^2+\frac{|\tilde{y}_i-\tilde{y}_j|^2}{\lambda^2}\Big) + \rho\sum_i(\tilde{x}_i^2+\tilde{y}_i^2)\Big). \tag{23}$$

The critical points of w, and thus the vortex positions, satisfy:

$$\rho\tilde{x}_i = \sum_{j\neq i}\frac{\lambda^2(\tilde{x}_i-\tilde{x}_j)}{\lambda^2|\tilde{x}_i-\tilde{x}_j|^2+|\tilde{y}_i-\tilde{y}_j|^2}\,, \tag{24}$$

$$\rho\tilde{y}_i = \sum_{j\neq i}\frac{\tilde{y}_i-\tilde{y}_j}{\lambda^2|\tilde{x}_i-\tilde{x}_j|^2+|\tilde{y}_i-\tilde{y}_j|^2}\,. \tag{25}$$

An immediate observation is that

$$\sum_i\tilde{x}_i = \sum_i\tilde{y}_i = 0\,. \tag{26}$$

By multiplying the equations with $\tilde{x}_i$ and $\tilde{y}_i$ respectively and adding the results together, one can obtain

$$\sum_i(\tilde{x}_i^2+\tilde{y}_i^2) = n(n-1)/(2\rho)\,. \tag{27}$$

Similarly, multiplying the equations with $\tilde{y}_i$ and $-\lambda^2\tilde{x}_i$ respectively and adding the results together, one gets

$$\rho(1-\lambda^2)\sum_i\tilde{x}_i\tilde{y}_i = 0\,. \tag{28}$$

Unlike equations (26,27) where the dependence on λ is implicit, the equation (28) leads to a property

$$\sum_i\tilde{x}_i\tilde{y}_i = 0\,, \quad \text{for } \lambda\neq 1\,. \tag{29}$$

The above observations lead to more precise predictions on the location of vortices.

For instance, in the case $n = 2$ we get $\tilde{x}_1 = -\tilde{x}_2$ and $\tilde{y}_1 = -\tilde{y}_2$. For $\lambda = 1$, we have an infinite set of solutions consisting in two points on the circle $\tilde{x}_i^2+\tilde{y}_i^2 = 1/\rho$, symmetric with respect to the origin. For $\lambda\neq 1$, (29) leads to $\tilde{x}_i\tilde{y}_i = 0$ for $i = 1, 2$, and we have a pair of solutions with either $\tilde{x}_i = 0$, $\tilde{y}_i = \pm\sqrt{1/2\rho}$, or $\tilde{y}_i = 0$, $\tilde{x}_i = \pm\sqrt{1/2\rho}$. Checking the corresponding values of w, we get that for $\lambda\neq 1$, the minimizer of w corresponds to having both vortices staying on the long-axis of the ellipse in the original scaling (that is on the x axis if $\lambda > 1$ and on the y axis if $\lambda < 1$). The estimate of the location is in agreement with the numerical solutions given later.

For the case $n = 3$, we also get that the 3 vortices are on the long-axis of the ellipse: one centered at the origin whereas the other pair stays symmetrically on the long-axis with $\tilde{x}_i = \pm\sqrt{3/2\rho}$ if $\lambda > 1$. Similar discussions can be carried out for other values of n. In general, for the case of n vortices, we let $R_1^2 = n(n-1)/2\rho$ and $\hat{x}_i = R_1\tilde{x}_i$, $\hat{y}_i = R_1\tilde{y}_i$. It follows from (27) that the points $\{\tilde{p}_i\}$ are localized by the minimum of

$$-\sum_{i\neq j}\log\Big(|\hat{x}_i-\hat{x}_j|^2+\frac{|\hat{y}_i-\hat{y}_j|^2}{\lambda^2}\Big).$$

under the constraint $\sum_i\hat{x}_i^2+\hat{y}_i^2 = 1$. It is reasonable to expect that this formula will lead to a vortex array as observed in [16]. Note that the minimizer $\{\hat{p}_i = R_1\tilde{p}_i\}$ has no explicit dependence on Ω, thus, we expect for a given λ, the vortex configuration to be of similar structure for values of Ω close to Ω_n. On the other hand, for a given n and Ω, we expect, however, that for sufficiently large λ, that is for highly anisotropic traps, the minimizer of w is given by the collinear solutions with vortices all located on the long axis of the elliptical trap.

To our knowledge, theoretical investigation had been restricted to the critical velocity for nucleation of one vortex. Here, we are able to deal with the case of multiple vortices and to precisely characterize the location of the vortices. Our estimates are also consistent with the numerical results given later.

IV. EVOLUTION EQUATION AND NUMERICAL SCHEMES

To numerically compute the energy minimizers of (5), we notice that the energy in (5) can be rewritten as

$$\int_{\mathcal{D}} \left\{ |(\nabla - i\mathbf{A})u|^2 + \frac{1}{2\varepsilon^2}(a_\varepsilon(\mathbf{r}) - |u|^2)^2 \right\} + c_\varepsilon \qquad (30)$$

where $a_\varepsilon(\mathbf{r}) = a(\mathbf{r}) - \varepsilon^2\Omega^2 r^2$,

$$\mathbf{A} = \begin{pmatrix} y \\ -x \end{pmatrix} \mathbf{\Omega}\,, \quad \text{and} \quad c_\varepsilon = \int_{\mathcal{D}} \{\frac{1}{2\varepsilon^2}(a^2(\mathbf{r}) - a_\varepsilon^2(\mathbf{r}))\}.$$

The above formulation of the energy has a striking similarity with the high-kappa high-field Ginzburg-Landau energy [17] with a variable coefficient [18].

A. Evolution in the imaginary time

To numerically compute the minimizers of (5), we consider the time-dependent equation in the imaginary time:

$$\frac{\partial u}{\partial t} - (\nabla - i\mathbf{A})^2\, u + \frac{1}{\varepsilon^2}|u|^2 u - \frac{a_\varepsilon(\mathbf{r})}{\varepsilon^2} u = \mu_\varepsilon(u) u \qquad (31)$$

in $\mathcal{D}$ with initial condition $u(\mathbf{r}, 0) = u_0(\mathbf{r})$ in $\mathcal{D}$ and boundary condition $u = 0$ on $\partial\mathcal{D}$. Here, $\mu_\varepsilon(u)$ denotes the Lagrange multiplier. Assume that u_0 satisfies the constraint $\|u_0\| = 1$. Then, by taking

$$\mu_\varepsilon(u) = \int_{\mathcal{D}} \left\{ |(\nabla - i\mathbf{A})\, u|^2 + \frac{1}{\varepsilon^2}|u|^4 - \frac{a_\varepsilon(\mathbf{r})}{\varepsilon^2}|u|^2 \right\} d\,\mathcal{D}\,,$$

we get

$$\frac{d}{dt}\left(\int_{\mathcal{D}} |u|^2 d\mathcal{D} - 1 \right) - \mu_\varepsilon(u) \left(\int_{\mathcal{D}} |u|^2 d\mathcal{D} - 1 \right) = 0\,.$$

Thus, the constraint $\int_{\mathcal{D}} |u|^2 = 1$ is ensured at all time. Moreover, using $(u, u_t) = 0$, we get the energy estimate:

$$\frac{1}{2}\frac{d}{dt}\mathcal{E}_\varepsilon(u) + \|\frac{\partial u}{\partial t}\|^2 = 0\,.$$

Thus, we easily get that for any $(0, T)$, if $u_0 \in H_0^1(\mathcal{D})$ and $\|u_0\| = 1$, there exists a unique strong solution u of (31) satisfying the constraint $\|u\| = 1$. Using argument similar to that in [21, 22], we may also get that as $t \to \infty$, u approaches to a steady state solution which is a critical point of the energy. Well-posedness for L^2 initial data may also be be obtained.

B. Numerical schemes

There are various ways to solve the time-dependent Gross-Pitaevskii equations, see for example [2] or [4]. We take the advantage of the striking similarity with the high-kappa high-field time-dependent Ginzburg-Landau equations [20], and adapt a code developed in [18, 19, 20]. Spatially, we use a standard finite element approximation, see [18, 19] for details. Here, we focus on the time-discretization and the treatment of constraint. It has been observed that there are some steady states exhibiting meta-stability, thus it is important to get asymptotically stable schemes for large time which in general requiring the use of implicit schemes with no limitations on the time step size.

Let $\{u_n\}$ be approximate solutions of $\{u(t_n)\}$ at discrete time $\{t_n\}$ with time-step $\Delta t_n = t_n - t_{n-1}$. We discuss two time-discretization schemes and also some results of numerical experiments.

c. A first order backward-Euler in time discretization Given u_{n-1}, we first solve for u^*:

$$\frac{u^* - u_{n-1}}{\Delta t_n} - (\nabla - i\mathbf{A})^2\, u^* - \mu(u_{n-1})u^* + \frac{1}{\varepsilon^2}|u^*|^2 u^* - \frac{1}{\varepsilon^2} a_\varepsilon u^* = 0 \qquad (32)$$

Then, we apply the projection $u_n = u^*/\|u^*\|$. Both the backward Euler step and the projection step gives only first order in time accuracy.

d. A norm-preserving, energy-decreasing second order scheme For any u, v and their complex conjugate $\bar{u}$, $\bar{v}$, we let $f(u, v) = (|u|^2 + |v|^2)(u + v)/2$ which satisfies $f(u, v)(\bar{u} - \bar{v}) = (|u|^4 - |v|^4)/2$. Given u_{n-1}, we first solve for u^*:

$$\frac{2(u^* - u_{n-1})}{\Delta t_n} - (\nabla - i\mathbf{A})^2\, u^* - \nu(u^*)u^* + \frac{1}{\varepsilon^2} f(2u^* - u_{n-1}, u_{n-1}) - \frac{1}{\varepsilon^2} a_\varepsilon u^* = 0 \qquad (33)$$

where $\nu(u^*)$ is given by

$$\nu(u^*) \int_{\mathcal{D}} |u^*|^2 = \int_{\mathcal{D}} \left\{ |(\nabla - i\mathbf{A})\, u^*|^2 \right\} + \int \left\{ \frac{1}{\varepsilon^2} f(2u^* - u_{n-1}, u_{n-1})\bar{u}^* - \frac{a_\varepsilon}{\varepsilon^2}|u^*|^2 \right\}\,.$$

Then we let $u_n = 2u^* - u_{n-1}$. Taking the inner product of the equation (33) with u^*, we get $(u^* - u_{n-1}, u^*) = 0$, which leads to $\|u_n\|^2 = \|u_{n-1}\|^2$. That is, the norm is preserved at each time step. Taking the inner product of the equation (33) with $u^* - u_{n-1}$, it is easy to get

$$2\frac{\|u_n - u_{n-1}\|^2}{\Delta t_n} + \mathcal{E}_\varepsilon(u_n) - \mathcal{E}_\varepsilon(u_{n-1}) = 0.$$

Thus, during the discrete time evolution, the energy decreases. This discrete scheme is second order in time and unconditionally stable. It also preserves some essential features of the continuous dynamic system, making it suitable for long time integration and for studies of meta-stabilities of the solutions.

C. Description of the numerical experiments

We have used the above schemes to calculate various numerical solutions for the parameter values $\varepsilon = 0.02$, $\lambda = 1$ and $\lambda = 1.5$. The spatial finite element space is taken to be C^0 piecewise quadratic elements on triangular meshes. As we are mostly interested in the minimizers of the Gross-Pitaevskii energy, the time-evolution is employed as a means of marching to the steady state solutions. For this reason, we have used variable time-steps in order to accelerate the convergence in time. The nonlinear systems are solved by a Newton like methods at each step. Though such a method is computational costly per step, this drawback is offset by its unconditional asymptotic stability for marching to the steady state. We have also computed the solutions using refined meshes to ascertain the numerical convergence.

To obtain solutions for various velocities, we have used a number of differential initial conditions. For example, we have used $|u_0(\mathbf{r})|^2 = a(\mathbf{r})$ for $\mathbf{r} \in \mathcal{D}$ which serves as a good approximation to the steady state solution, especially in the case of vortex-free solutions. We note that for large values of Ω, this choice of initial condition can also lead to steady state solutions with multiple vortices. Detailed solution branches are described in the next section. In addition, we have also used other initial conditions that manually *plant* vortices in the domain in order to find different solution branches. Finally, a continuation in the parameter Ω has often been employed to follow a particular solution branch and to compute the bifurcation diagrams. The continuation procedure also provides a test for the local stability of the numerical solutions: when one branch becomes unstable, the solution jumps onto a different branch.

V. NUMERICAL RESULTS AND BIFURCATION DIAGRAMS

We now present some pictures of numerical solutions and discuss the various solution branches.

A. Description of solutions

e. The case of a disc For any Ω, there is a vortex free solution, which is close to $a(x, y)$ except near the boundary. For $\Omega = 0$, in addition to this vortex free solution, there is also a one vortex solution, as illustrated in the first column of Figure 1.

For larger Ω, solutions with multiple vortices are shown in the other columns of Figure 1. For instance, solutions with 2 and 3 vortices for $\Omega = 15$ are shown in the second column, solutions with 4 and 5 vortices for $\Omega = 17.5$ are shown in the third column, and solutions with 6 and 7 vortices for $\Omega = 20$ are shown in the last column. The parameter values for which the single-vortex and multi-vortices solutions exist are to be presented in the next section. Figures 2 and 3 provide the surface plots (and better view) of $|u|$ for a vortex free solution at $\Omega = 0$ and a solution at $\Omega = 20$ with four vortices respectively. Each solution has a top and bottom view, the paraboloid shapes are easy to visualize from the picture.

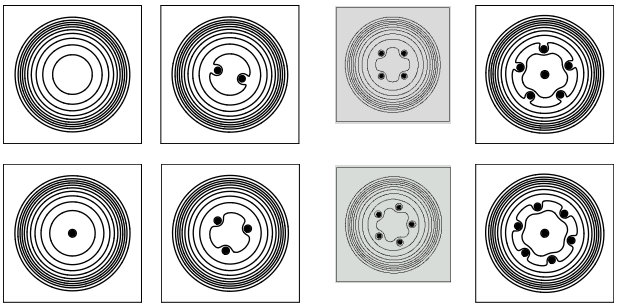

FIG. 1: Contour plots of $|u|$ for $\Omega = 0$ (1st column), 15 (2nd column) 17.5 (3rd column) and 20 (4th column).

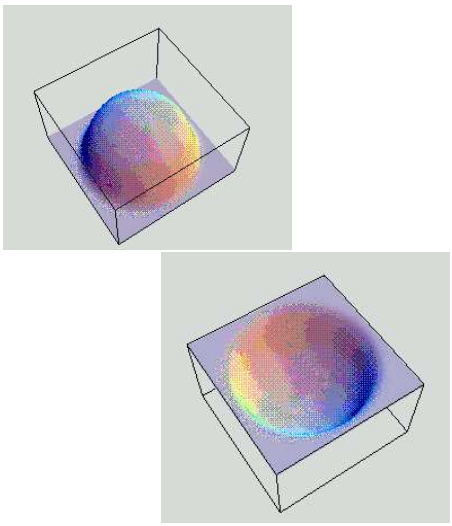

FIG. 2: Surface plots of $|u|$ for solutions at $\Omega = 0$.

f. The case of an ellipse We now present some solutions for an ellipse corresponding to $\lambda = 1.5$. In Figure 4, the contour plots of the magnitude of the solution $|u|$ with $\Omega = 17.5$ are drawn while in Figure 5, $\Omega = 25$. For $\Omega = 17.5$, it is interesting to compare the location of vortices with the analysis of section III.c: in this case $\rho = 0.79$, the long axis is 0.9887 and we find for the location of the vortex $x = 0.19$ for $n = 2$ and $x = 0.33$ for $n = 3$. The picture shows that the vortex is about $1/5$ of the long axis for 2 vortices and $1/3$ for 3 vortices, which is consistent with the analysis. We believe that for a bigger number of vortices n, their location corresponds to the positions minimizing (23).

Note that there were two vortex configurations with five vortices for $\Omega = 25$, among which, the non-symmetric configuration corresponds to a solution with a lower free energy, though the difference in their energy values is very small.

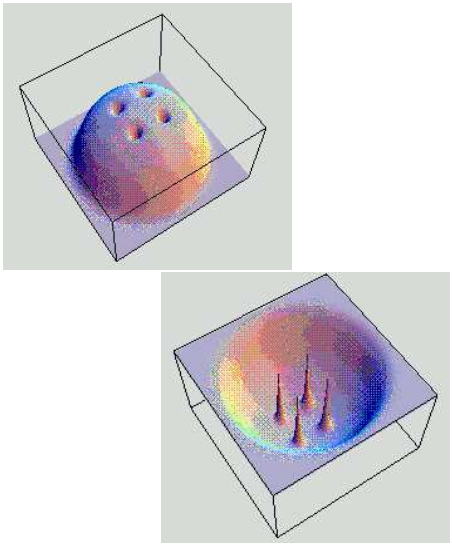

FIG. 3: Surface plots of $|u|$ for solutions at $\Omega = 20$.

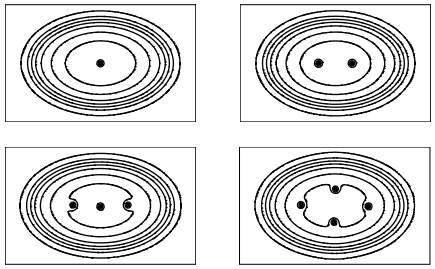

FIG. 4: Contour plots of $|u|$ for $\Omega = 17.5, \lambda = 1.5$

B. Branches of solutions

An issue that we have studied is the existence of branches of n vortex solutions as Ω is varied and especially which one is the minimizer.

g. The case of the disc For $\Omega = 0$, the solution with lowest energy is the vortex free solution. We start with this solution as initial value for the time dependent problem for a slightly bigger Ω. This device allows us to continue the branch of the vortex free solution as Ω is increased. We find that the vortex free solution is obtained as the limit when t is large of the evolution equation up to $\Omega = 19$. For $\Omega = 19$, six vortices are nucleated from the boundary and eventually one vortex moves to the center and final configuration is similar to that in Figure 1 (top right). Now if Ω is decreased from the value 19 using the 6 vortices solutions as initial value, we see that this 6 vortices solution branch exists down to $\Omega = 16$ when it jumps to 4 vortices. If we decrease Ω further, then we stay on the 4 vortex branch down to $\Omega = 13$ when it drops to a 2 vortex branch. Similarly, if we increase Ω from 13, the 2 vortices solution will persist up to $\Omega = 21$.

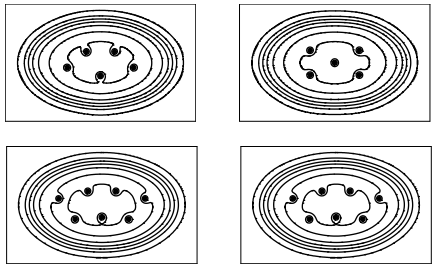

FIG. 5: Contour plots of $|u|$ for $\Omega = 25, \lambda = 1.5$

As for the one-vortex solution branch, it is computed by planting a vortex-like function at the center in the initial condition for $\Omega = 10$, then the branch is computed by continuation in Ω (both increasing and decreasing). It is interesting to observe the fact that this branch extends all the way to $\Omega = 0$, such persistence of the one-vortex solution even for the zero velocity has been elaborated by various authors, see [4] for instance. Since implicit integration is used, we are able to indeed march to to the steady state and to ascertain that this persistence is not due to the metastability. On the other hand if the vortex is planted away from the origin, it disappears for small Ω as we will see later.

h. The case of an ellipse The same kind of behaviour occurs for the vortex free solution branch with $\lambda = 1.5$: when Ω is increased from 0, we stay on the vortex free branch up to $\Omega = 22.5$ when the solution jumps to the 4 vortex branch of Figure 5. If we decrease Ω starting from this 4 vortex branch, the solution will stay on it down to $\Omega = 15$ when it jumps to 2 vortices and at $\Omega = 10$ it jumps to the vortex free solution. Similarly to the case of the disc, if one vortex is planted at the center at time 0, it will persist in time even down to $\Omega = 0$.

For Ω large enough, several vortices are nucleated at the same time. Basically, we are counting on initial conditions and the round-off errors to break the symmetry of the region and strong symmetry presence often makes symmetry breaking much harder to achieve. For the disc case, we expect equal chance of vortex nucleation from any point of the boundary. It turns out that for $\Omega = 19$, an unstable front produces oscillations of almost equal magnitude, and spins off 6 vortices at the same time. Had the disturbance being unevenly distributed, then it would be possible for some vortices to get spin off ahead of others, and due to the repulsion, the others may never have a chance to appear, thus we may see solutions with a smaller number of vortices.

C. Energy diagrams

We now discuss the energy diagrams in relation to the discussion of the critical velocities given in the earlier sections. In Figures 6 and 7, we have plotted the energy given by (3) as a function of Ω for the various branches of solutions (according to the number of vortices). Again, $\varepsilon = 0.02$ in our computation.

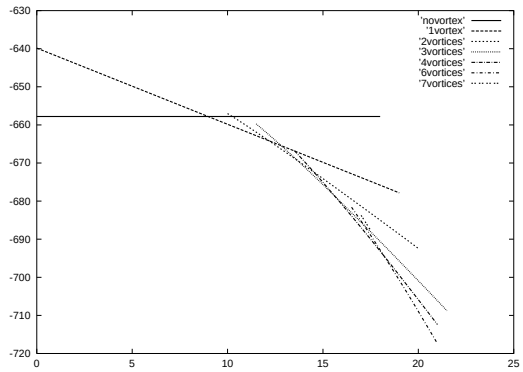

FIG. 6: The energy vs. Ω curves for $\lambda = 1.0$

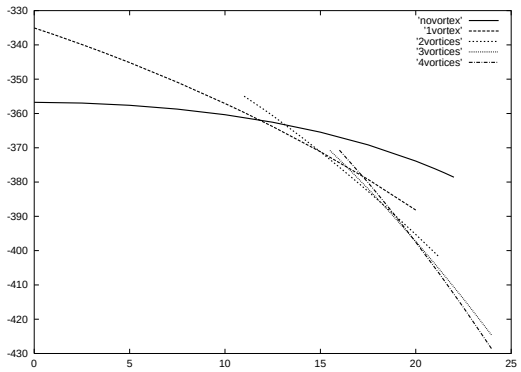

FIG. 7: The energy vs. Ω curves for $\lambda = 1.5$

i. The case of the disc (Figure 6) As discussed earlier, the vortex-less solution, in the case of the disc, exists for all values of Ω and is independent of Ω, we thus have a constant line for its energy. These vortex-free solutions are the global energy minimizers for small Ω ($\Omega < 9.3$) whereas for $\Omega > 9.3$, they have larger energy than the one-vortex solution. For multi-vortex solutions, we see that each becomes the global energy minimizer for a range of values of Ω. It is interesting to compare this result with the value found in section 2 where $\Omega_1 = 9.8$. Similarly, we obtain from (22) that $\Omega_n - \Omega_{n-1} \simeq 1.77$. Though the value of Ω_1 is slightly overestimated, the difference $\Omega_n - \Omega_{n-1}$ looks good for small n: the numerics indicate $\Omega_2 = 12.0$, $\Omega_3 = 13.6$, $\Omega_4 = 15.8$ and our theoretical computations yield $\Omega_2 = 11.6$, $\Omega_3 = 13.4$, $\Omega_3 = 15.2$.

However, when Ω is increased from 0, we saw that we stay on the vortex free branch up to $\Omega = 19$. This means that the vortex free solution is a local minimizer up to this value. We do not have any theoretical estimate for this value of local minimum. Similarly, for multi-vortex solutions, hysteresis loops are present. For the solution with six vortices, there are two possible configurations, one with all six on a concentric circle, one with only five on a concentric circle while the remaining vortex at the center of the disc. This occurs for $\Omega = 22.5$. Though the difference in the energy is hardly noticeable, the solution with a center vortex does have a smaller energy value.

j. The case of an ellipse (Figure 7) Now, we discuss the elliptical case with $\lambda = 1.5$. The energy versus Ω curves are given in Figure 7.

The vortex-less solution, in the case of the ellipse, is no longer independent of Ω as in the case of the disc, as illustrated by the dependence its energy on Ω. Aside from that, the hysteresis phenomena also occurs just like for the case of a disc.

Our numerics indicate that $\Omega_1 = 12$, $\Omega_2 = 15$. It is interesting to compare this result with the value found in section 2: we obtain that $\Omega_1 \simeq 13$ from (22) that $\Omega_n - \Omega_{n-1} \simeq 2.88$. Though the value of Ω_1 is slightly overestimated, the difference $\Omega_n - \Omega_{n-1}$ looks good again since we find $\Omega_2 = 14.9$.

D. Displacement of the vortex from the center

Based on the earlier estimate (19) for the one-vortex solution, we see that for small Ω, the displacement of the vortex away from the center leads to the drop of energy ($\Omega < 4.9$). For slightly bigger Ω a vortex at the center is a local minimum ($\Omega < 9.8$). Let us analyze the time dependent equation using a vortex off center as initial condition and let us examine how it evolves. We find that in the case of the disk, for $\Omega < 7$, a displacement on the size of a tenth of the radius causes the displaced center vortex in the one-vortex solution to move towards the boundary. For $\Omega > 10$, the center vortex in the one-vortex solution moves back towards the center if under a displacement on the size of a third of the radius. For intermediate values of Ω, the vortex moves back to the center for small displacement but moves towards boundary for large displacement.

The following two pictures (Figures 8 and 9) show, in the case of a disc and a small displacement, the marching away of the center vortex for the solution with $\Omega = 0$ (starting from top row then to the bottom row) and the marching back to the center for the solution with $\Omega = 7.9$.

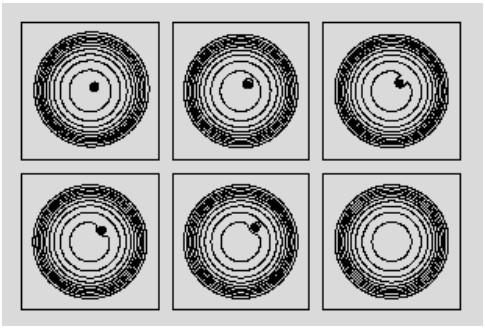

FIG. 8: Perturbing vortex away from center for $\Omega = 0$

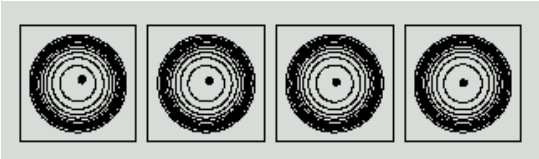

FIG. 9: Perturbing vortex away from center for $\Omega = 7.9$

VI. CONCLUSION

We have presented a new framework for the study of the Gross Pitaevskii energy in the Thomas Fermi limit: we have defined a nondimensionnalized parameter ε and we have computed theoretically an asymptotic development of the energy, the critical thermodynamic velocities of nucleation of vortices and the location of vortices. This extends the results of [2]. We have proposed and implemented time integration schemes which enjoy the norm-preserving and energy-descreasing features and thus useful for studying the stability and metastability of solutions. We have also presented energy diagrams computed numerically for the various vortex solutions. We have noticed that our theoretical predictions for critical thermodynamic velocities are quite consistent with the numerics which encourages us to think that our approximation ε small is correct though $|\log \varepsilon|$ is not small.

In our computation, we have taken $\varepsilon = 0.02$ and the number of vortices we have observed ranges from 0 to 10 for Ω between 0 and 25.

Our aim for a future work is to use the results of [23] for Ginzburg-Landau in dimension 3 to get results for rotating Bose Einstein condensates in dimension 3, and especially the critical velocities and an asymptotic development of the energy. In particular, it is obtained in [8] that $\Omega_s = 3/5\Omega_1$ for a vortex line parallel to the z axis, but we would like to get an expression of the energy for any type of vortex line. We will also carry out further numerical simulations in 3 dimension to compare with experimental data.

Acknowledgments

The authors would like to thank Y.Castin for very interesting discussions and also T.Riviere, E.Sandier, S.Serfaty. This work is supported in part by a joint France-Hong Kong research grant.

[1] D.Butts and D.Rokhsar, Nature **397**, 327 (1999).
[2] Y.Castin and R.Dum, Eur. Phys. J. D, **7**, 399 (1999).
[3] F.Dalfovo, S.Giorgini, L.Pitaevskii and S.Stringari, Rev. Mod. Phys. **71**,463 (1999).
[4] D.L.Feder, C.W.Clark and B.I.Schneider, Phys. Rev. Lett., **82**, 4956 (1999).
[5] A.L.Fetter, Phys. Rev A, **148**, 429 (1965).
[6] A.L.Fetter and A.A.Svidzinsky, cond-mat/0102003.
[7] K. Madison, F. Chevy, W. Wohlleben and J. Dalibard, Phys. Rev. Lett., **84**, 806 (2000).
[8] A.A.Svidzinsky and A.L.Fetter, Phys. Rev. Lett., **84**, 5919 (2000).
[9] F.Dalfovo, L.Pitaevskii and S.Stringari, Phys. Rev. A **54**, 4213 (1996).
[10] A.L.Fetter and D.L.Feder, Phys. Rev. A, **58**, 3185 (1998).
[11] A.Aftalion, E.Sandier and S.Serfaty, to appear in J. Math. Pures et Appl. (2000).
[12] S. Serfaty, *Comm. Contemporary Mathematics, 1*, 213 and 295 (1999).
[13] S.Serfaty, to appear in Control, Optimization and Calculus of Variations (2001).
[14] F. Bethuel, H. Brezis and F. Helein, *Ginzburg-Landau Vortices*, (1994) Birkhäuser.
[15] F. Bethuel and T. Riviere, Annales IHP, Analyse non linéaire, **12**, 243 (1995).
[16] D.L.Feder, C.W.Clark and B.I.Schneider, Phys. Rev. A, **61** 011601(R) (1999).
[17] S. Chapman, Q. Du, M. Gunzburger and J. Peterson, Adv. Math.Sci. Appl. **5**, 193 (1995).
[18] Q. Du, M. Gunzburger and J. Peterson, Phys. Rev. B, **46**, 9027 (1992); Q. Du, M. Gunzburger and J. Peterson, Phys. Rev. B, **51**, 16194 (1995).
[19] Q. Du, M. Gunzburger and J. Peterson, SIAM Review, **34**, 54 (1992).
[20] Q. Du, P. Gray, SIAM Appl Math, **56**, 1060 (1996).
[21] F. Lin, Q. Du, SIAM Math Anal, **28**, 1265 (1997).
[22] L. Simon, Annals of Math **118**, 525 (1983).
[23] F.Pacard and T.Riviere, in Progress in Nonlinear Differential Equations and their Applications, **39** Birkhäuser Boston, Inc., Boston, MA, 2000.